Novel experimental concept for high frequency multi-axial fatigue analysis of cylindrical specimens

B. Van Hooreweder[1], D. Moens[1], R. Boonen[1], P. Sas[1]
[1]Department of Mechanical Engineering (PMA), K.U.Leuven, Celestijnenlaan 300b, B-3001 Leuven, Belgium
email: brecht.vanhooreweder@mech.kuleuven.be

ABSTRACT: This paper describes the development of a novel experimental concept for high frequency multi-axial fatigue analysis of cylindrical specimens. The resulting test rig applies a combination of bending and torsional stress to test specimens with critical diameters ranging from 2 to 15mm at test frequencies up to 50Hz. Furthermore, the amplitude and frequency of both loadcases can be controlled independently. This enables the use of a broad range of test conditions. Test data will be generated which can be used to study and validate multi-axial fatigue criteria for synchronous and asynchronous loading conditions. Furthermore, the test rig will be used to study the effect of size on the fatigue life of metal and plastic components.
The test setup consists of a closed mechanical loop which is driven by an electromotor. The primary shaft contains the cylindrical test specimen and is modified to impose rotating bending loads. The secondary shaft is adjusted to introduce fluctuating torque in the transmission loop. Both shafts are connected by means of two double link mechanisms to minimize the clearance and the inertia of the system. The time-varying multi-axial stress state in the cylindrical specimen is analyzed as a function of the amplitudes and frequencies of both bending and torsional loadcases. This is verified by a numerical fatigue analysis in MSC-Patran and MSC-Fatigue. Finally the dynamical behavior of the test rig is studied using a 5 DOF torsional mass-spring representation and the Lagrangian method. A more complex model with 20 DOF is implemented in SimDriveLine and solved via Matlab to analyze the kinematical and dynamical properties more accurately. Both studies take the mechanical properties of steel or plastic test specimens of different size into account.

KEY WORDS: Fatigue test rig; Multi-axial loading; Torque introducing concept.

1 INTRODUCTION

Various mechanical components such as driveshafts, windturbine propeller blades, suspension parts, machine components, etc. are subjected to multi-axial fluctuating loading conditions. This results in complex stress-strain distributions at critical locations of the geometry. Fatigue analysis of these components can be done with traditional analytical and numerical techniques using an equivalent uni-axial loadcase [1]. This way, the standardized material data from Wöhler's rotating bending tests can still be used to evaluate the fatigue strength.

The state of stress and strain becomes even more complicated when asynchronous loading conditions with variable amplitude are applied. A large number of theories [2-5] is available to determine equivalent uni-axial loading conditions for synchronous loadings. Additional research using experimental methods is necessary to improve the knowledge of the fatigue phenomena under asynchronous conditions. Therefore, a new experimental concept is developed.

2 NOVEL EXPERIMENTAL CONCEPT

2.1 Requirements

Some requirements for the multi-axial fatigue test rig are listed in Table 1. The experimental setup should allow testing of steel and plastic cylindrical components of different diameters under multi-axial loading conditions. The high test frequency (<50Hz) allows for accelerated fatigue experiments on metals while the low test frequency (>2Hz) enables tests on polymers without heat dissipation. To allow all possible loading combinations, fluctuating bending and torsional stresses have to be introduced using two independable exciter systems. In addition, it is desirable to come to a straightforward experimental concept that is economically feasible using commercially available components. Finally, the concept should be conform the relevant standards for introducing bending and torsional stress [6-7].

Table 1. Test rig requirements.

Requirement	Value
Torsional moment	5 – 200 [Nm]
Bending moment	5 – 150 [Nm]
Test frequency	2 – 50 [Hz]
Diameter specimens	2 – 15 [mm]

2.2 Concept

The concept of the experimental setup is based on the back-to-back closed transmission loop as used in the FZG test rig (Figure 1) for gear strength evaluation [8].

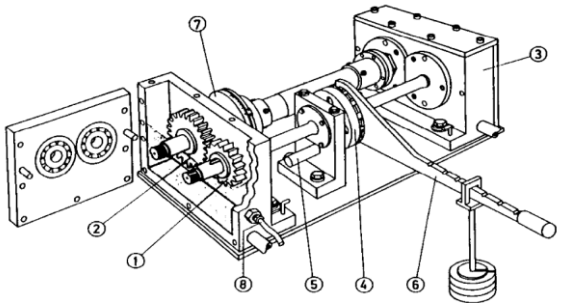

Figure 1. FZG gear test rig.

The lever (6) is used to lock a constant torque in the closed loop prior to testing. Because of the closed loop, the motor connected to one of the shafts only needs to provide a limited amount of energy which is equal to the energy losses in the two gearboxes and the bearings.

The presented concept uses the same closed loop principle as shown in Figure 2. The motor is connected with a flexible joint (1) to the primary shaft (6) that contains the cylindrical test specimen (4). The secondary shaft (8) is driven by two identical gearboxes (5) and contains a torque introducing device (7).

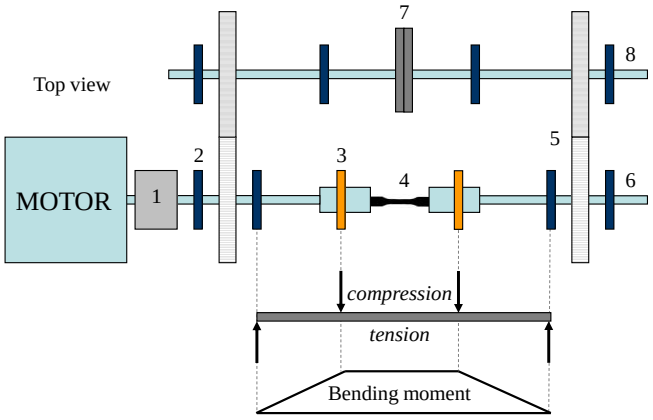

Figure 2. Concept of the test setup.

Fluctuating bending stress is introduced on the test specimen by applying the rotating four point bending principle. Two self aligning ball bearings (3) can move on a linear slider in the horizontal plane. By adjusting the position of these two inner bearings, a pure bending moment is introduced as shown in the lower diagram in Figure 2. Consequently, a rotating shaft leads to alternating tension and compression stresses on the test specimen.

Fluctuating torsional stress is introduced by means of two identical planetary gear boxes (7) as indicated in Figure 3. The carriers of both gearboxes are connected. Ring gear 1 is fixed to the ground and ring gear 2 is attached to a lever arm which is connected to an electrodynamic shaker. If the lever arm is standing still, 'sun 1' and 'sun 2' experience the same rotational speed. Excitation of the lever arm causes the transmission ratio of the second gearbox to change, leading to a relative rotational speed difference between 'sun 1' and 'sun 2' and a variable torque in the closed transmission loop.

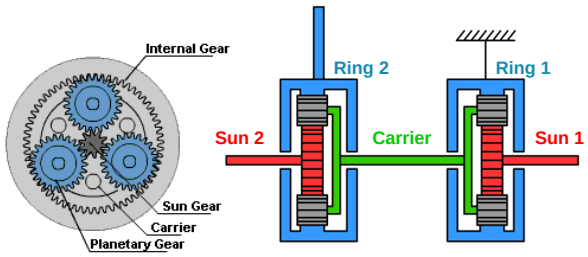

Figure 3. Planetary gearboxes to introduce fluctuating torque.

Since bending and torsion are introduced be means of two separate exciters, both in-phase and out-of-phase loading with constant or variable amplitude is possible at two different excitation frequencies.

2.3 *Validation of scaling laws for mechanical fatigue*

The presented test rig can be used to clamp specimens of different length and diameter using an adapted ER40 tool holder and different collets. By doing so, the effect of specimen size on the fatigue life of different materials under various loading conditions can by studied and scaling laws can be validated using the approach as illustrated in Figure 4.

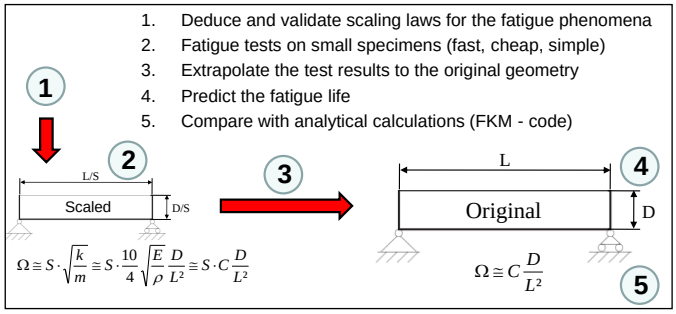

Figure 4. Study of size effects for mechanical fatigue.

If properly defined, scaling laws can be used to predict the fatigue life of large scale structures by performing accelerated tests on small scale models and by extrapolating these results [9]. Fatigue experiments on small models are easier to set up and more time and cost effective than tests on large models. Furthermore the test frequency can be increased due to the higher first eigenfrequency (Ω). Scale effects are also important to consider when fatigue data of standardized, small test pieces is used to predict the fatigue life of real components.

3 STRESS ANALYSIS OF TEST SPECIMEN

3.1 *Local stress analysis*

The applied bending moment is constant over the entire length of the test specimen. Taking the specimen as a reference, the bending moment vector M rotates with respect to the specimen at angular velocity ω_B. Figure 5 shows a cross section of the specimen with position vector P and the bending moment vector M at time t = 0 (a) and t = t_1 (b).

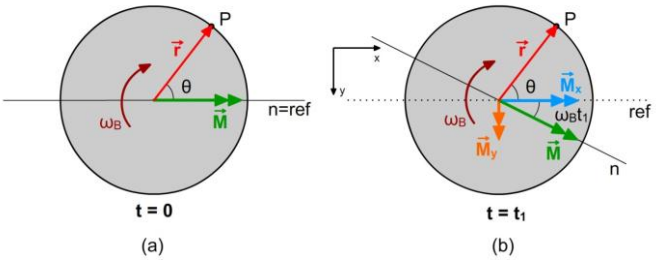

Figure 5. Rotating bending moment vector (M) and position vector (P) in cross-section of material sample.

The bending moment can be decomposed in a coordinate system fixed to the specimen in two time-varying components M_x and M_y. In combination with a fluctuating torsion load the time-dependent load of the specimen consist of the following components:

$$M_x(t) = M\cos(\omega_B t) \quad (1)$$

$$M_y(t) = M\sin(\omega_B t) \quad (2)$$

$$T(t) = T\sin(\omega_T t + \emptyset) \quad (3)$$

ω_B and ω_T are the angular velocities and M and T are the amplitudes of the bending and the torsional moment. Φ is the phase angle between both moments. By using these equations, the combination of rotating bending and fluctuating torsion loading can be simulated numerically using the finite element method on a fixed geometry with three time varying load vectors. In general, normal and shear stress in any point P(r,θ) can be calculated as follows.

$$\sigma_{B,P}(t) = \frac{Mr}{I_n}\sin(\omega_B t + \theta) \quad (4)$$

$$\tau_{T,P}(t) = \frac{Tr}{I_P}\sin(\omega_T t + \emptyset) \quad (5)$$

3.2 Global stress analysis

The phase difference (θ - Φ) between bending and torsion does not influence the way the specimen is loaded. Altering this phase difference results in the same cyclic stress state, but shifted angularly across the section. The angular velocities ω_B and ω_T on the other hand, have a strong influence on the loading condition. When both angular frequencies are equal ($\omega_B = \omega_T = \omega$), a component of the bending load is in phase with the torsional load. This is illustrated in Figure 6 where the coordinate system xy (Figure 5) is rotated over an angle equal to Φ resulting in a new coordinate system x'y', where $M_{y'}(t)$ is in phase or proportional with T(t) and were $M_{x'}(t)$ is 90° out-of-phase.

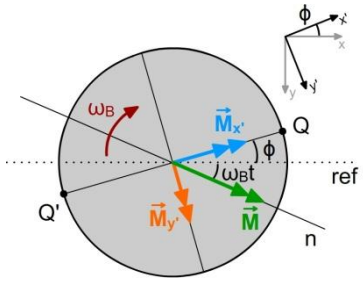

Figure 6. Decomposition of M in x'y'.

Subsequently, formula (1), (2) and (3) can be rewritten as:

$$M_{x'}(t) = M\cos(\omega_B t + \emptyset) \quad (6)$$

$$M_{y'}(t) = M\sin(\omega_B t + \emptyset) \quad (7)$$

$$T(t) = T\sin(\omega_T t + \emptyset) \quad (8)$$

Since the neutral lines (n) always coincide with the bending moment vectors, it can be seen that the normal stress is only proportional with the shear stress when $M_{x'}(t) = 0$ (line Q-Q'). Hence the maximum absolute values of the principal stresses will occur in points Q and Q' twice each rotation. In these points the relation between normal and shear stress is constant.

$$\frac{\sigma_B(t)}{\tau_T(t)} = \frac{MI_P}{TI_n} = \frac{2M}{T} \quad (9)$$

This proportional state of stress was validated using a 3D finite element model of the geometry, MSC.Patran as pre- and postprocessor and the MSC.Fatigue solver [11]. Rotating bending and fluctuating torsion were applied on a fixed specimen according to formulas (1), (2) and (3). The quadratic tetraëder mesh was refined until bending and torsional stress converged to the results of formula (4) and (5). Figure 7 shows the fatigue life of FEM-nodes on the critical circumference of the test specimen. Minimal fatigue life is obtained for two nodes with angular difference of 180° (points Q and Q' in Figure 6). In these nodes bending and torsional stresses reach their maximum values during each cycle. For all other nodes on the circumference, the maximum values of bending and torsion are shifted in phase and fatigue life is higher.

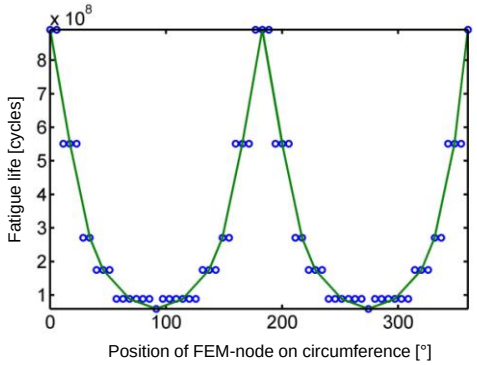

Figure 7. Fatigue life of FEM-nodes on critical circumference.

If $\omega_B \neq \omega_T$ non proportional loading occurs. When the torsional moment reaches a maximum absolute value, two points on the circumference exist where the bending stresses are also maximum in tension or compression. Generally, these points are not located at fixed positions on the test specimen as the experiment continuous. In addition, two specific cases can be analyzed.

- If $\omega_T > \omega_B$, at least two times per revolution a maximum absolute value of principal stress is reached. Furthermore, if $\omega_T = n\omega_B$ (n = 2,3,..) the circumference of the section has 2n fixed highly loaded points.
- If $\omega_B > \omega_T$, at most two times per revolution a maximum absolute value of principal stress is reached. Furthermore, if $\omega_B = n\omega_T$ (n = 2,3,..) the highly loaded points occurs every n revolution.

3.3 Stress trajectories

Stress trajectories are lines in a stress field whose tangents are principal directions of the state of stress. They can be found analytically (using Mohr's circle), numerically (finite element method) or experimentally (photoelasticity). Analysis of the trajectories brings insight in complex states of stress and highly loaded areas [12].

For the cylindrical test specimen (Figure 8a), the trajectories are analyzed for the unfolded surface area because fatigue failure is most likely to initiate at the surface of the specimen. For a pure bending load on the cylindrical specimen only normal stress would occur leading to horizontal trajectories. When pure torsion is applied, the trajectories would cross each other at an angle of 90°, the angle between the centerline and the trajectories being 45°.

A combination of bending and torsion results in trajectories as indicated by Figure 8b. On the right, the principal stresses and the stresses in a cylindrical coordinate system are indicated on infinitesimal elements. The blue lines represent the direction of compression stress and the red lines the

direction of tensile stress. On the neutral lines (N_1, N_2) only the influence of torsion is noted while all other horizontal lines show both the influence of bending and torsion. In the upper part, where tensile stresses are present due to the bending moment, the positive principal stress (red) aligns more with the axial (x) direction. In the lower part, where compressive stresses are present, the negative principal stress (blue) aligns more with the axial direction.

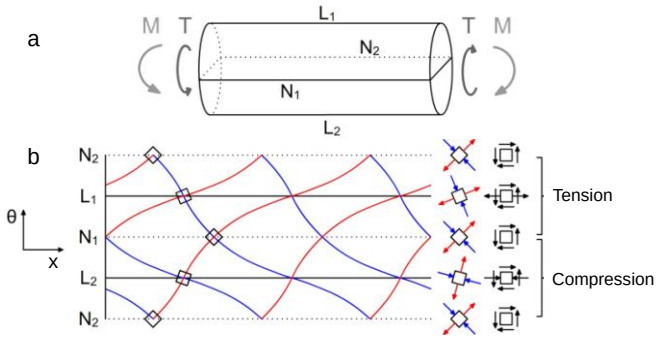

Figure 8. Cylindrical test specimen (a) and stress trajectories (b).

4 DYNAMIC BEHAVIOR OF THE TEST RIG

4.1 Methodology and results

The study of the dynamic behavior of the test rig is important to limit the influence of unbalance and resonance in bending or torsion on the loading of the test specimen and the fatigue life of the test rig. In the rotating test setup specimens of different size and material can be used. This causes the dynamic properties of the whole system to change depending on the mass and stiffness properties of the clamped test specimen. In order to deal with this efficiently, the torsional vibrations of the test rig are analyzed using a simple model with 5 rotational DOF as indicated in Figure 9. All mechanical components are represented by their inertia (J_i) and rotational stiffness (k_i) values. The subscripts 'R', 'S' and 'C' refer to the ring, sun and carrier of the planetary gearbox.

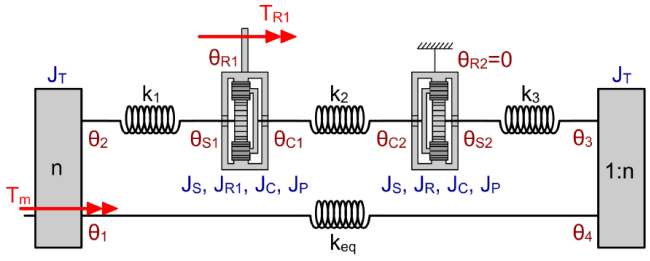

Figure 9. 5 rotational DOF representation of the test rig.

The static torque on the test specimen (T_{SP}) can be calculated using formula (10) where n and g are the transmission ratios of the conventional and planetary gearbox respectively and T_{R1} represents the torque input on the ring gear.

$$T_{SP} = k_{eq}(\theta_4 - \theta_1) = \frac{n}{g} T_{R1} \;;\; g = \frac{r_R}{r_S} \qquad (10),(11)$$

The relation between the rotational variables in Figure 9 can be formulated using the formulas (12), (13) of the planetary gearboxes [13] leading to 5 DOF: θ_1, θ_4, θ_{S1}, θ_{R1}, θ_{S2}.

$$\dot{\theta}_2 = n\dot{\theta}_1 \;;\; \dot{\theta}_3 = n\dot{\theta}_1 \;;\; \dot{\theta}_3 = n\dot{\theta}_4 \;;\; \dot{\theta}_{C1} = \left(\frac{g\dot{\theta}_{R1} + \dot{\theta}_{S1}}{1+g}\right) \qquad (12)$$

$$\dot{\theta}_{P1} = \left(\frac{g\dot{\theta}_{R1} - \dot{\theta}_{S1}}{g-1}\right) \;;\; \dot{\theta}_{C2} = \left(\frac{\dot{\theta}_{S2}}{1+g}\right) \;;\; \dot{\theta}_{P2} = \left(\frac{-\dot{\theta}_{S2}}{g-1}\right) \qquad (13)$$

The equations of motion of this model are calculated analytically using the method of Lagrange [14]. The Lagrangian (L) of the system is calculated as function of the kinetic and potential energy.

$$L = E_{KIN} - E_{POT}$$
$$= \frac{1}{2}\left[\begin{array}{c} J_T\dot{\theta}_1^2 + J_T\dot{\theta}_4^2 + J_{R1}\dot{\theta}_{R1}^2 + J_S\dot{\theta}_{S1}^2 + J_S\dot{\theta}_{S2}^2 + J_{CP}\left(\frac{g\dot{\theta}_{R1} + \dot{\theta}_{S1}}{1+g}\right)^2 \\ +pJ_P\left(\frac{g\dot{\theta}_{R1} - \dot{\theta}_{S1}}{g-1}\right)^2 + J_{CP}\left(\frac{\dot{\theta}_{S2}}{1+g}\right)^2 + pJ_P\left(\frac{-\dot{\theta}_{S2}}{g-1}\right)^2 \end{array}\right]$$
$$-\frac{1}{2}\left[\begin{array}{c} k_{eq}(\theta_1 - \theta_4) + k_1(n\theta_1 - \theta_{S1})^2 + k_2\left(\frac{g\theta_{R1} + \theta_{S1} - \theta_{S2}}{1+g}\right)^2 \\ +k_3(\theta_{S2} - n\theta_4)^2 \end{array}\right] \qquad (14)$$

This formula is then solved for every DOF using the Lagrange equation (Formula 15), leading to 5 equations of motion.

$$\frac{d}{dt}\left(\frac{\partial L}{\partial \dot{\theta}_i}\right) - \frac{\partial L}{\partial \theta_i} = T_i \qquad (15)$$

The equations of motion are reformulated using modal transformation, leading to a global inertia matrix [M] and stiffness matrix [K].

$$[M][\ddot{\theta}] + [K][\theta] = 0 \qquad (16)$$
$$(-\underline{M}\omega^2 + \underline{K})\theta = 0 \qquad (17)$$
$$(\underline{M}^{-1}\underline{K} - \lambda\underline{I})\theta = 0 \;;\; \lambda = \omega^2 \;;\; f_n = \frac{1}{2\pi}\sqrt{\lambda} \qquad (18)$$

The undamped eigenvalues and eigenvectors are calculated in Matlab by solving Formula 18 for the smallest and most flexible specimen in steel. Table 2 shows the first 3 natural frequencies with normalized modal shapes for every variable grouped per rotational stiffness (k_i). Variables (θ_i) that depend on the 5 DOF of the system are also calculated and displayed in gray.

Table 2. Eigenvalues and normalized eigenvectors.

DOF	$f_{n,1}$ = 0Hz	$f_{n,2}$ = 33Hz	$f_{n,3}$ = 445Hz	k_i
θ_1	0,5	0,482	0.179	k_{eq}
θ_4	0,5	-0,476	-0.179	
θ_2	0,5	0,482	0,179	k_1
θ_{S1}	0,5	0,502	-0.917	
θ_{C1}	-0,1	-0,0969	0,0584	k_2
θ_{C2}	-0,1	-0,0956	-0,0132	
θ_{S2}	0,5	-0,478	-0.0661	k_3
θ_3	0,5	-0,476	-0,179	
θ_{R1}	0	-0,247	0.302	

At $f_{n,1}$ = *0Hz*, a rigid body mode is present. All the shafts rotate at fixed speeds determined by the transmission ratios n and g without deflections/vibrations. The DOF have the same amplitude and phase except for the ring gears that are standing still.

At $f_{n,2}$ = *33Hz*, the first flexible body mode is present. The primary shaft (Figure 2) with the test specimen is clearly the most deforming element as can be seen on the out-of-phase movement of θ_1 and θ_4 with relative high amplitudes in comparison with other mode shapes.

At $f_{n,3}$ = *445Hz*, the second flexible body mode is present. The left part of the secondary shaft (k_1) is now the most deforming element. The other natural frequencies $f_{n,4}$ and $f_{n,5}$ are far above the testing frequencies.

To study the test rig more in detail, a parametric Simulink model is created and Matlab is used to implement the parameters and run the model [15]. To start with, the 5 DOF system is build using the components from SimDriveLine to represent the gearboxes and shafts (Figure 10). The input of the model is a torque impuls (T_{R1}) on one ring gear so that all eigenfrequencies of the system are excited. The outputs of the model are the rotational speeds ω_i which are integrated to find the rotational DOF θ_i. The torque on the test specimen T_{SP} is calculated using Formula 10.

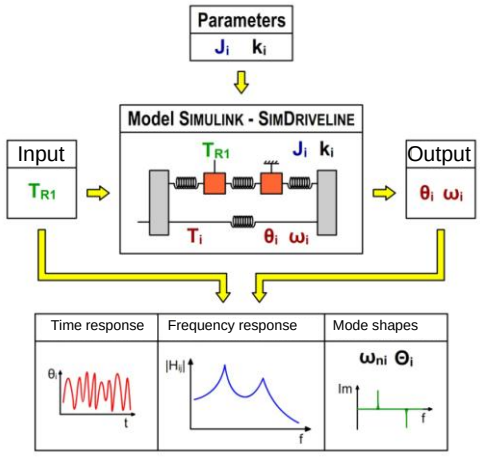

Figure 10. Simulation of dynamic behavior.

To study the dynamic behavior of the test rig, the frequency response function H between T_{R1} and T_{SP} is calculated in Matlab after discrete Fourier transformation of the windowed time signals. The result is shown on a semilogarithmic scale in Figure 11. In this case the 0Hz mode is not excited because of the impuls on the ring gear.

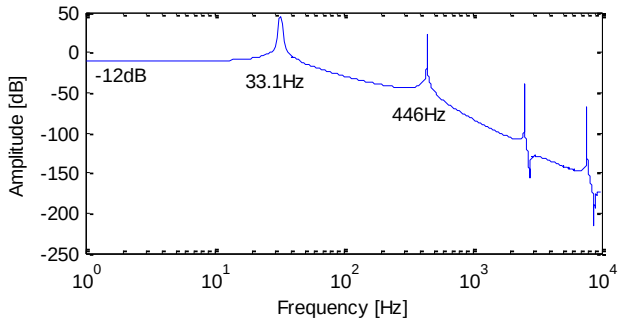

Figure 11. Frequency response function of T_{SP} and T_{R1}.

The system response at 0Hz corresponds to the transfer of a static torque on the ring gear to a static torque on the test specimen. This can be validated using the gearbox transmission ratios n and g.

$$\frac{T_{SP}}{T_{R1}} = \frac{n}{g} \rightarrow |H|_{dB} = 20log_{10}\left(\frac{n}{g}\right) = -12dB \qquad (19)$$

Furthermore, all natural frequencies show good correlation with the frequencies calculated analytically. Hence, the Simulink model was validated and used to model the test rig more in detail by introducing torsional spring-damper-clearance elements to study the influence of backlash in the gearboxes on the torque distribution of the test specimen in the time domain. Additionally, the rotating parts of the test rig were simulated more accurately by dividing them in smaller parts and modeling these with more spring and inertia elements. The resulting model with 20 DOF allows calculation of the higher torsional eigenfrequencies. In addition, the gear mesh frequencies are calculated by multiplying the number of teeth with the rpm of each gear in the transmission loop. To avoid higher vibration modes, the test frequencies can be altered so that the gear-mesh frequencies do not excite the higher eigenfrequencies of the test setup.

4.2 Interpretation of results

It is clear that for the initial design of the test rig, the first eigenfrequency in torsion (33Hz) is within testing range (2-50Hz) leading to resonance and high vibration amplitudes when testing the smallest or the most flexible specimen in steel. Moreover, above the first natural frequency, force controlled testing is difficult because the system's response depends on the inertia rather than the stiffness values. This dynamic behavior can be partially improved by increasing the stiffness k_1 and k_3 and decreasing the inertia moments J_i. The influence of the inertia of the ring gear (J_{R1}) and the inertia of the connection between primary and secondary shaft (J_T) on the first eigenfrequency is studied using sensitivity analysis. The result is shown in Figure 12 where M represents the multiplication factor that is applied to the inertia values. Halving both J_{R1} and J_T results in an increase of the first eigenfrequency from 33.1Hz to 50Hz. Design modifications to address this are discussed further in '§5'.

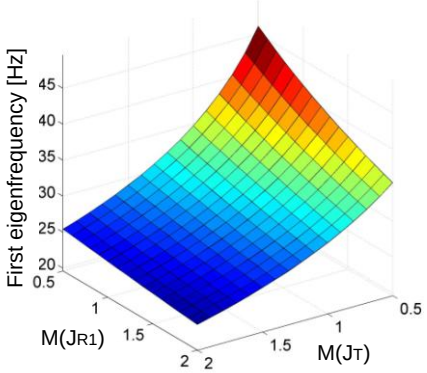

Figure 12. Sensitivity analysis

When the steel specimen is replaced by polymer specimens, the rotational eigenfrequencies change to a frequency range between 6 and 18Hz. This is feasible because fatigue experiments on polymers should be performed at low frequencies, typically 1-3Hz, to avoid temperature accumulation during the experiment.

5 DESIGN MODIFICATIONS

Figure 13 illustrates the final design of the test rig. A speed controlled synchronous motor (1) drives the test rig via a torsionally flexible jaw type joint (2). To reduce clearance and unbalance and to guarantee perfect alignment, three identical customized bearings housings (4) are designed to fit the bearings of the primary and secondary shaft. For the four point rotating bending, two smaller bearing housings (5) are mounted on a linear slider mechanism. Adjustment in the x-direction (10) is necessary for mounting and demounting of the test specimens (9). Adjustment in the y-direction (11) allows for bending of the specimen in the xy-plane. This is feasible because of the self-aligning ball bearings in (5) and the bellow-type joints (7) which are torsionally stiff but allow for angular deflection in the xy-plane.

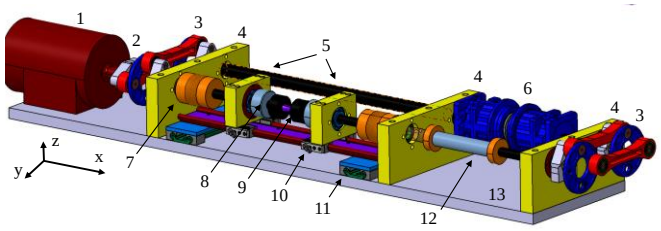

Figure 13. Final design of the test rig

The primary and the secondary shaft are connected by means of a double four link mechanism (3) as shown more in detail in Figure 14. In comparison with the original gearboxes, this lowers the inertia (J_T) by a factor 1.8. To neutralize the effect of discontinuities in the torque transfer, two horizontal links are used with a 90° phase difference. To align the mechanism with the shafts, two self centering clampex joints are used.

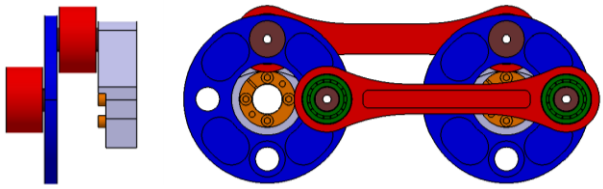

Figure 14. Side and front view of double four link mechanism

To cope with high radial forces (6kN) at high speeds (50Hz) and to limit the dimensions and inertia of the mechanism, double row full complement cylindrical roller bearings are used. The angular clearance (θ_c) of this mechanism is only function of the radial internal play in the cylindrical roller bearings, leading to a decrease in clearance by a factor 26.7.

$$\theta_{c,gearbox} = 8\ arcmin. \tag{20}$$

$$\theta_{c,mechanism} = \frac{z}{r} = \frac{3e^{-9}mm}{50mm} = 0.3\ arcmin. \tag{21}$$

The test specimen (9) is clamped in two modified straight shaft ER40 tool holders. Collets with variable inner diameter (3-26mm) can be used to clamp specimens of different dimensions with high accuracy. On each tool holder, an incremental encoder is mounted in order to perform displacement-controlled torsional loading on the specimen. Furthermore, a wireless torque sensor (12) is implemented for force-controlled fatigue testing. The bending is introduced by means of springs in the linear slider (11) which can be preloaded with a bolt and measured with force cells.

According to Figure 12 the inertia (J_{R1}) of the components to introduce fluctuating torque (6) should lower by at least a factor 2. This is not possible by using commercially available planetary gearboxes hence a new concept is designed based on helical gears as illustrated in Figure 15. The upper part is integrated in the closed mechanical loop and connected via shafts a_1 and a_2. These shaft are free to rotate at different angular speeds due to the axial thrust bearing (c) in the middle. Two sets of helical gears (b,e) are installed to drive shaft (f) which is journalled in hydrostatic bearings that also function as hydraulic pistons (d). Axial movement of shaft (f) from '1' to '2' leads to CCW rotation of shaft (a_1) and CW rotation of shaft (a_2) as indicated in the right part of the figure. The relative angular difference ($\Delta\theta$) of both shafts causes torque on the test specimen. Similarly, axial excitation will cause fluctuating torque on the test specimen.

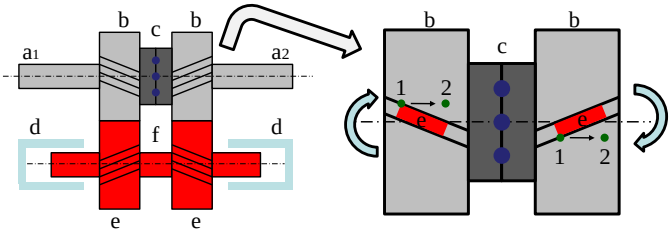

Figure 15. Torque introduction by means of helical gears

The required angular difference ($\Delta\theta$) to apply a certain torque (T) on the test specimen is calculated using the Simulink model of the test rig. Then the tangential displacement (x_t) of the gears and the axial displacement (x_a) of the shaft can be calculated as function of $\Delta\theta$, the gear radius (r) and the helix angle (β). The gear contact forces are calculated to design the gears for the worst-case-scenario, e.g. large test specimen diameter and high testing speed.

$$x_t = \frac{\Delta\theta}{2} r = 0.97mm\ ;\ x_a = \frac{x_t}{\tan\beta} = 2.08mm \tag{22}$$

$$F_t = \frac{T}{r} = 4164N\ ;\ F_a = F_t \tan\beta\ ;\ F_r = \frac{F_a}{\cos\beta} \tag{23}$$

Using these forces, the tooth-root strength and the contact strength is analyzed for commercially available gears. Grinded helical gears from case hardened ground steel with toothing quality 7e25 (m = 3, z = 20, r = 70mm) offer sufficient strength for low weight, leading to a total inertia reduction of 2.3 with respect to the double planetary gearboxes.

6 CONCLUSIONS

A multi-axial fatigue test rig is designed to subject cylindrical test specimens of different size and material to bending and torsional stresses up to 50Hz. The test rig is based on the closed loop concept. Fluctuating bending stresses are applied using rotating four point bending. Fluctuating torsional stresses are introduced using axial excitation of a third shaft with helical gears. Since both loadcases can be controlled independently, the concept allows for a broad range of testing

conditions that are relevant for real life applications such as drive shafts loaded in bending and torsion. Furthermore, stress analysis is performed so that proportional and non-proportional rotating bending and torsion can be easily implemented in finite element fatigue calculations.

The analytical calculation of the dynamic behavior of the test rig shows good correlation with the simulation in SimDriveLine. Using these results, the initial design of the test rig is altered to avoid excitation of the torsional eigenfrequencies. The conventional gearboxes are replaced by two double link mechanisms leading to minimal clearance and a decrease in inertia by a factor 1.8. Furthermore, the planetary gearboxes are replaced by a new principle for the introduction of torque in the loop using helical gears. In the final design, the first eigenfrequency of the test rig increased from 33.1 to 50 Hz for the smallest and most flexible test specimen in steel. Specimens of polymer materials yield lower eigenfrequencies but should be tested below 3Hz to avoid temperature accumulation.

ACKNOWLEDGMENTS

This research is funded by a Ph.D grant of the Institute for the Promotion of Innovation through Science and Technology in Flanders (IWT-Vlaanderen).

REFERENCES

[1] E. Zahavi, V. Torbilo. Fatigue Design: Life Expectancy of Machine Parts. CRC press, 1996.
[2] N.E. Dowling. Mechanical behaviour of materials: Engineering Methods for Deformation, Fracture, and Fatigue. Pearson Prentice Hall, 2007.
[3] D.F. Socie, G.B. Marquis. Multiaxial Fatigue. SAE International, 2000.
[4] Miller, Brown. Multiaxial fatigue. ASTM special technical publication; 853, 1985.
[5] FKM-guideline, Analytical Strength Assessment of Components in Mechanical Engineering, VDMA, 5th revised edition, 2003.
[6] ISO 1143 and DIN 50113, Rotating bar bending Fatigue Testing.
[7] ISO 1352, Torsional stress fatigue testing.
[8] DIN ISO 14635-1, Gears, FZG test procedures, 2006.
[9] Van Hooreweder B, Sas P, Boonen R, Moens D, De Coninck F, Experimental investigation of scaling laws for mechanical fatigue behaviour. In: 8th National Congress on Theoretical and Applied Mechanics 8.8, pp. 659–663, 2008.
[10] G. Van der Linden, J. Vercammen, B. Van Hooreweder, D. Moens, Analysis of a multi-axial fatigue test rig implementation, K.U.leuven, 2010.
[11] MSC.Fatigue user's manual, nCode International, 2005.
[12] F. Thamm, The role of the stress trajectories as an aid in the choice of the suitable shape of load-bearing structural elements of engines and structures, Periodica Polytechnica, Ser. Mech. Eng. Vol 44, No. 1, p171-183, 2000.
[13] F. L. Litvin, A. Fuentes, Gear Geometry and Applied Theory. Cambridge University Press, 2004.
[14] D. Wells, Lagrangian Dynamics, Schaum's outline series. McGraw-Hill, New York, 1967.
[15] The MathWorks, SimDriveLine, model and simulate the mechanics of driveline systems, 2004.